Water Science and Engineering 2016, 9(1): 3−13

Available online at www.sciencedirect.com

Water Science and Engineering

journal homepage: http://www.waterjournal.cn

Comparison between wave generation methods for numerical simulation of bimodal seas

Daniel A. Thompson*, Harshinie Karunarathna, Dominic Reeve

Energy & Environment Research Group, Zienkiewicz Centre for Computational Engineering, Swansea University, Bay Campus, Swansea SA1 8EN, UK

Received 31 May 2015; accepted 16 November 2015
Available online 3 March 2016

Abstract

This paper describes an investigation of the generation of desired sea states in a numerical wave model. Bimodal sea states containing energetic swell components can be coastal hazards along coastlines exposed to large oceanic fetches. Investigating the effects of long-period bimodal seas requires large computational domains and increased running time to ensure the development of the desired sea state. Long computational runs can cause mass stability issues due to the Stokes drift and wave reflection, which in turn affect results through the variation of the water level. A numerical wave flume, NEWRANS, was used to investigate two wave generation methods: the wave paddle method, allowing for a smaller domain; and the internal mass source function method, providing an open boundary allowing reflected waves to leave the domain. The two wave generation methods were validated against experimental data by comparing the wave generation accuracy and the variance of mass in the model during simulations. Results show that the wave paddle method not only accurately generates the desired sea state but also provides a more stable simulation, in which mass fluctuation has less of an effect on the water depth during the long-duration simulations. As a result, it is suggested that the wave paddle method with active wave absorption is preferable to the internal wave maker option when investigating intermediate-depth long-period bimodal seas for long-duration simulations.

Keywords: Wave modeling; Wave generation; RANS; Swell wave; Bimodal sea; Long-period waves

1. Introduction

Low-pressure storm systems in the deep ocean can generate waves with enough energy to enable them to travel away from the wave generation area and towards the shoreline. These waves, commonly known as swell waves, have the characteristics of long periods, low frequencies, and long wavelengths. Due to the longer wavelengths, swell waves have a greater runup and are therefore more likely to overtop coastal structures than others. This has significant impacts across the globe; flooding as a result of swell waves has been observed (Draper and Bownass, 1982; Turton and Fenna, 2008; Sibley and Cox, 2014). Occasionally extensive flooding occurs when a storm travels across an ocean at a sufficient velocity to maintain an input of energy into the longer-period wave group (Sibley and Cox, 2014). This was likely the case during the United Kingdom's winter storms of 2013−2014, when a successive run of severe low-pressure Atlantic storms caused extensive damage and flooding along the coastline. During cases of severe damage and flooding, wave periods greater than 20 s were observed (Slingo et al., 2014).

This paper examines the problem of generating bimodal swell waves in a numerical flume in order to further investigate their effects on coastal structures. A bimodal sea state occurs when both low-frequency swell waves and high-frequency local wind-generated waves are present at the same location. A significant problem when dealing with long-period waves is the increase of wavelength. This requires

This work was supported by the Natural Environment Research Council as part of a PhD studentship (Grant No. EGF406).
* Corresponding author.
E-mail address: 555157@swansea.ac.uk (Daniel A. Thompson).
Peer review under responsibility of Hohai University.

http://dx.doi.org/10.1016/j.wse.2016.02.005

larger modeling domains, both in physical models and numerical simulations, to prevent reflected waves from the shoreline from reaching the wave generation region. For intermediate- to deep-water waves, the longer wavelengths mean that the wave can travel at a faster speed and can therefore be reflected more easily if the nearshore slope structure allows. Reducing the amount of reflection is important as it can affect the initial wave generation. In nature, an open boundary naturally occurs, which absorbs waves reflected by the coastal system. A wave flume is a closed system, and any reflected wave from the shoreline will be re-reflected in the wave generation area, thus altering the wave characteristics at the shoreline (Frigaard and Brorsen, 1995). Ideally, absorption measures need to be in place to ensure that re-reflection does not occur. The long-period waves investigated in this study make reflected waves more likely, thereby making absorption more difficult. In numerical flumes, the re-reflected wave can also cause an increase in the mean water level (Higuera et al., 2013; Torres-Freyermuth et al., 2010). During long-duration simulations this can become significant and will decrease the accuracy of the simulation.

In investigation of bimodal seas, the model running time is important. Sufficient time is required for the sea state to fully develop so as to ensure that all frequencies are represented in a test. This study used experimental data to compare the accuracy in wave generation with two different methods. The wave paddle method has been used extensively in numerical flume applications (e.g., Lin and Liu, 1998; Reeve et al., 2008; Jones et al., 2013; Zou et al., 2013), with good results. The internal mass source function method has also been used in numerical flume applications (e.g., Lin and Liu, 1999; Lara et al., 2010; Wei et al., 1999). To the best of the authors' knowledge there has been no comparison of the two in terms of generating bimodal seas with desired swell components and for long computational runs. Hafsia et al. (2009) provide a comparison between the wave paddle and mass source function methods, but only for solitary wave generation, finding that both methods perform equally well in comparison with experimental data. When the internal wave maker was developed for the NEWRANS model, Lin and Liu (1999) compared the generation of different wave types (i.e., irregular, second-order, and linear) and found good agreement with analytical solutions. However, the irregular wave test comprised the superposition of only three different wave frequencies, providing a very coarse representation of a full spectrum.

The aim of this study was to validate the NEWRANS model's capabilities in generating bimodal seas through comparison of simulated waves with experimental data. The long-duration simulations required allowed the effects of wave reflection to be analyzed through observation of increases in water level. This paper begins with a brief introduction of the model and a more extensive overview of the theory and application of the two wave generation methods. Next, the model setup and the data used for validation are introduced and explained. Results from the comparisons between the model results and experimental data are presented, along with a discussion of the role of relative water depth and beach slopes in wave generation. This is followed by concluding remarks.

2. Numerical model and wave generation methods

2.1. Model formulation

In this work, a two-dimensional (2D) numerical flume was used to investigate two wave generation procedures. The numerical flume, NEWRANS (Lin and Liu, 1998), was based on the Reynolds-averaged Navier-Stokes (RANS) equations and uses a volume-of-fluid capturing scheme to allow for accurate simulation of large deformations during wave breaking and overtopping. NEWRANS calculates the free surface and general turbulent flow by decomposing the flow in the model into the mean flow and turbulent fluctuations. As a result, a set of equations is determined for the mean flow containing contributions from the fluctuating turbulent flow. To describe the effects of these fluctuations on the mean flow, the model is coupled with a second-order k-ε turbulence closure model.

For turbulent flow, both the velocity field and pressure field are split into mean components ($\overline{u}_i$ and $\overline{p}$) and turbulent fluctuations (u_i' and p'). Thus, $u_i = \overline{u}_i + u_i'$ and $p = \overline{p} + p'$. Once substituted into the Navier-Stokes equations, the mean flow is governed by the RANS equations:

$$\frac{\partial \overline{u}_i}{\partial x_i} = 0 \tag{1}$$

$$\frac{\partial \overline{u}_i}{\partial t} + \overline{u}_i \frac{\partial \overline{u}_i}{\partial x_i} = -\frac{1}{\rho}\frac{\partial \overline{p}}{\partial x_i} + g_i + \frac{1}{\rho}\frac{\partial \overline{\tau}_{ij}}{\partial x_j} - \frac{\partial \overline{u_i' u_j'}}{\partial x_j} \tag{2}$$

where the subscripts i and j are equal to 1 or 2, representing the two directions in the Cartesian coordinate system; u_i is the ith component of the velocity vector; ρ is the density of the fluid; g_i is the ith component of the gravitational acceleration; t is the time; and $\overline{\tau}_{ij}$ is the viscous stress tensor of the mean flow. The Reynolds stress is modeled by an algebraic nonlinear Reynolds stress model (Shih et al., 1996):

$$\begin{aligned}\rho \overline{u_i' u_j'} = {} & \frac{2}{3}\rho k \delta_{ij} - C_\mathrm{d}\rho \frac{k^2}{\varepsilon}\left(\frac{\partial \overline{u}_i}{\partial x_j} + \frac{\partial \overline{u}_j}{\partial x_i}\right) - \\ & \rho \frac{k^3}{\varepsilon^2} C_1 \left(\frac{\partial \overline{u}_i}{\partial x_l}\frac{\partial \overline{u}_l}{\partial x_j} + \frac{\partial \overline{u}_j}{\partial x_l}\frac{\partial \overline{u}_l}{\partial x_i} - \frac{2}{3}\frac{\partial \overline{u}_l}{\partial x_m}\frac{\partial \overline{u}_m}{\partial x_l}\delta_{ij}\right) + \\ & C_2\left(\frac{\partial \overline{u}_i}{\partial x_m}\frac{\partial \overline{u}_j}{\partial x_m} - \frac{1}{3}\frac{\partial \overline{u}_l}{\partial x_m}\frac{\partial \overline{u}_l}{\partial x_m}\delta_{ij}\right) + \\ & C_3\left(\frac{\partial \overline{u}_m}{\partial x_i}\frac{\partial \overline{u}_m}{\partial x_j} - \frac{1}{3}\frac{\partial \overline{u}_l}{\partial x_m}\frac{\partial \overline{u}_l}{\partial x_m}\delta_{ij}\right)\end{aligned} \tag{3}$$

where C_d, C_1, C_2, and C_3 are empirical coefficients; δ_{ij} is the Kronecker delta (equal to 1 if $i = j$, and 0 if $i \neq j$); k is the turbulent kinetic energy, where $k = u_i' u_i'/2$; ε is the dissipation rate of turbulent kinetic energy, and $\varepsilon = \nu\overline{(\partial u_i'/\partial x_j)^2}$, where ν is the molecular kinematic viscosity: $\nu = \mu/\rho$, where μ is the dynamic viscosity; and l and m follow the Einstein tensor notation for summation. Lin and Liu (1998) determined the coefficients in Eq. (3) as follows:

$$C_d = \frac{1}{3}\left(\frac{1}{3.7+S_{max}}\right) \quad C_1 = \frac{1}{185.2+D_{max}^2}$$
$$C_2 = \frac{1}{58.5+D_{max}^2} \quad C_3 = \frac{1}{370.4+D_{max}^2} \tag{4}$$

where $S_{max} = \frac{k}{\varepsilon}\max\left|\frac{\partial \overline{u}_i}{\partial x_i}\right|$ and $D_{max} = \frac{k}{\varepsilon}\max\left|\frac{\partial \overline{u}_i}{\partial x_j}\right|$. A detailed description of the model is given in Lin and Liu (1998).

2.2. Wave generation methods

2.2.1. Wave paddle method

The velocity and free surface value are specified on the wave boundary based on the selected wave theory (i.e., linear, second-order Stokes, or cnoidal). This method is accurate in generation of waves from deep to intermediate water depths. The problem that arises from specifying the velocity and free surface in the wave paddle method is the same as that experienced in laboratory flumes. Reflected waves that reach the paddle position can degrade the wave generation signal due to re-reflection from the wave generating boundary. A way of avoiding this problem is using the paddle displacements directly from laboratory experiments involving active wave absorption. Torres-Freyermuth (2007) modified the wave maker mode to allow free-surface displacement and a velocity profile to be directly fed into the model. This means that the model can be fed using the laboratory measurements, analytical solutions, or numerical results. However, this approach can cause significant mass to be introduced into the computational domain due to the Stokes drift (i.e., asymmetrical free-surface velocities over one wave period, resulting in more fluid moving in the wave direction under the crest than under the trough) during long computational runs. To compensate for the potential increase in mass, a compensation procedure used in Torres-Freyermuth et al. (2007) is applied to the free-surface displacement and velocity profile. The procedure involves computing the relative mass evolution from the free-surface elevation time series and velocity profile of the desired input. A fourth-order polynomial fit is made of the observed mass oscillation and the difference between the fit and the instantaneous mass is computed for every time step. The difference is considered to be the time-evolution mass compensation required in order to achieve the mass balance at the end of the computation. The mass compensation required is then uniformly distributed from the bottom to the mean water levels as an undertow contribution according to the instantaneous free-surface elevation and velocity profile. Following that, the initial computed wave-induced velocity is modified by linearly superimposing the newly computed velocity. The model is then fed by the free-surface elevation time series and the computed velocity profile.

2.2.2. Internal mass source function method

The second method used in this study was the internal mass source function method, which was originally developed by Lin and Liu (1999). The concept is that any specific wave train can be generated using the mass source function of the equation of mass conservation in the internal flow region. This method is very useful for long-duration simulations in which reflected waves are significant (Soliman, 2003), because it removes the difficulty of the wave paddle method having to specify and react to reflected waves; a sponge layer or open boundary allows outgoing waves. A detailed description of the generation of different wave types with the internal mass source function method can be found in Lin and Liu (1999). The generation of irregular waves will be described below.

The model represents an irregular wave train by superposition of a finite number of linear wave modes, n, with different wave heights and wave frequencies using the following mass source function $S(t)$:

$$S(t) = \sum_{i=1}^{n} \frac{C_i H_i}{A}\sin(\sigma_i t - p_{si}) \tag{5}$$

where A is the area of the source region, and C_i, H_i, σ_i, and p_{si} are the speed, height, angular frequency, and phase angle of the ith wave mode, respectively. Lin and Liu (1999) suggest that, for a known energy spectrum of an irregular wave train, the inverse Fourier transformation be used to reconstruct the wave train with a finite number of wave modes. In this study, a method based on the procedure used by Lara et al. (2006) was used. Fig. 1 presents the process used to produce a series of linear waves to drive the internal wave maker to form a desired bimodal sea state, where S_i is the spectral density corresponding to the center of gravity of the energy band in the frequency band (f_i, f_{i+1}), and the dashed boxed area highlights the additional steps used in this study.

3. Results

3.1. Experimental setup

In order to validate the two wave generation methods, a series of laboratory data were used to drive the model with the aim of checking the model's capability of producing the same irregular wave trains and maintaining an acceptable variance in mass during the simulations. The experiments were performed as part of a Standing Conference on Problems Associated with the Coastline (SCOPAC)-funded project to investigate the response of a gravel beach to the effects of bimodal seas with increasing peak wave periods and swell components. The flume was 100 m long and 1.8 m wide, with a varying slope at a 1:25 scale. Waves were generated using a piston-type electric wave maker with active wave absorption. There were in total eight gauges along the flume, P1 to P8, as illustrated in Fig. 2. Each gauge collected data at 32 Hz for 1663 s. Wave sequences at peak wave periods T_p of 15, 21, and 25 s containing swell component percentages P_{sc} of 0%, 20%, 30%, and 40% were used to validate the model. Fig. 3 features the spectral shape of the bimodal waves generated in the physical flume. The generated waves were predominately intermediate water waves ($0.05 < d/L < 0.75$, where d is the water depth and L is the wavelength).

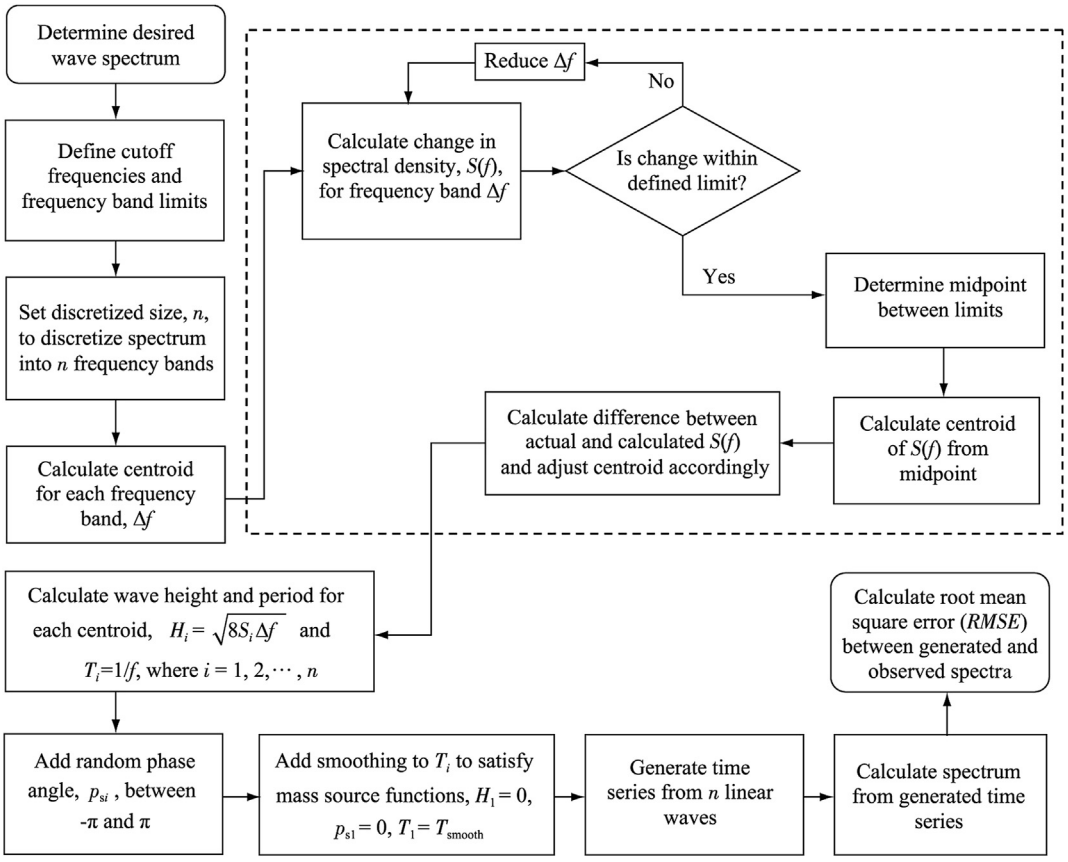

Fig. 1. Irregular wave generation procedure using internal mass source function method.

3.2. Model setup

A computational domain was designed to reproduce the laboratory data shown in Fig. 2. The setup fully represents the flume in terms of its length, depth, and beach slope. The grid system is uniform in both x- and y-directions. To properly capture breaking waves, the mesh resolution had to be very high and was therefore computationally expensive, with $\Delta y = 0.026$ m and $\Delta x = 0.048$ m. The computational domain was 2.05 m high. Therefore, a total of 80 cells were used in the y-direction. For the wave paddle method, the domain was 86.51 m long, with 1800 cells. When the internal mass source region is used, the length of the flume is dependent on the wavelengths of the waves produced; the distance between the mass source region and the open boundary needs to be at least half a wavelength to prevent unwanted artificial reflections (Lin and Liu, 1999). Therefore, for $T_p = 15$ s and 21 s, the flume was 111.51 m long and had 1940 cells in the x-direction ($\Delta x = 0.0575$ m); for $T_p = 25$ s, the flume was 121.51 m long and had 2100 cells in the x-direction ($\Delta x = 0.0579$ m). Fig. 4 demonstrates these dimensions, including the varying sizes and location of the source region. The wavelength and source region sizes in these tests were determined from the peak wave period of the test case and followed the rules as those defined in Lin and Liu (1999).

3.3. Model data comparison

3.3.1. Accuracy of wave generation methods

To demonstrate the accuracy of the two wave generation methods in generating a specific sea state, the spectra between the observed data and the simulated data were compared at wave gauge P1. Fig. 5 shows an example input when $T_p = 21$ s and $P_{sc} = 30\%$ from a 27-min simulation (duration of the physical tests). It is noticeable that the internal mass source function method does not produce the exact desired spectrum

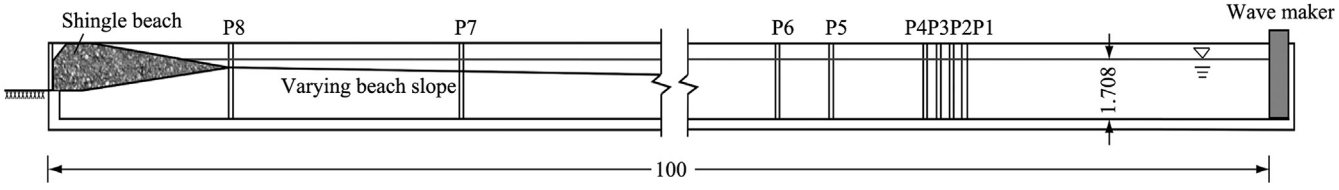

Fig. 2. Experimental setup (units: m).

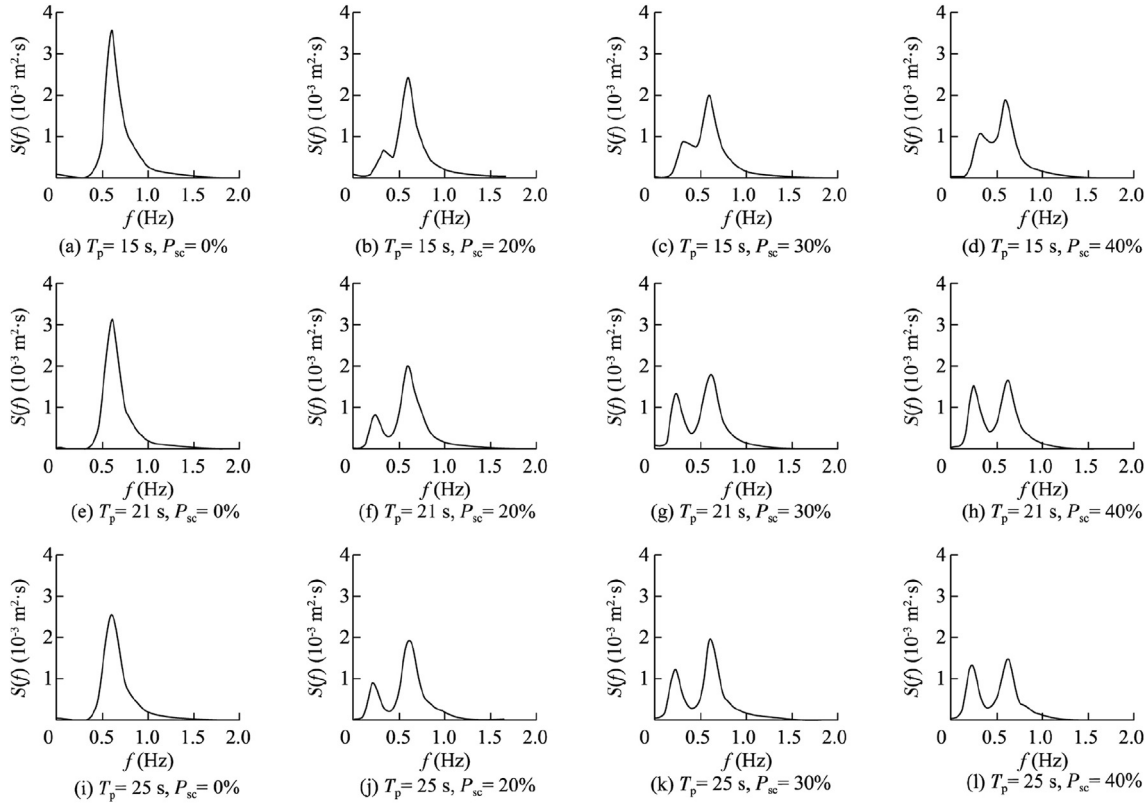

Fig. 3. Spectral shape of experimental data for each peak period and swell component percentage used as input for beach slope tests.

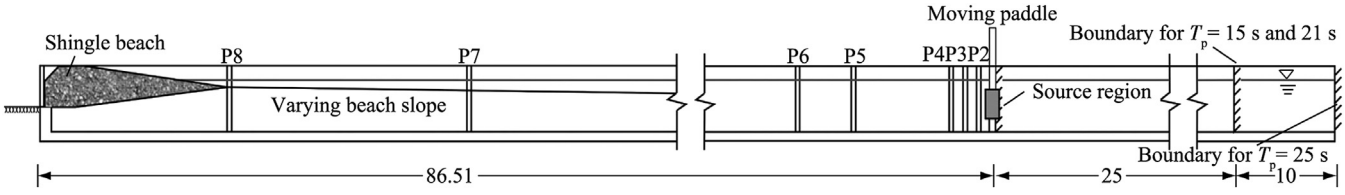

Fig. 4. Model setup (units: m).

and seems to lose energy as frequency increases. The spectra were compared for all test cases and the root mean square error (*RMSE*) was calculated between the observed and simulated values, as summarized in Fig. 6. It is clear from Fig. 6 that the paddle method produces a more accurate representation of the desired spectrum, whereas the internal mass source function method is less accurate. There is no discernible trend between the *RMSE* values and peak periods. However, wave generation accuracy seems to improve as the swell component percentage increases.

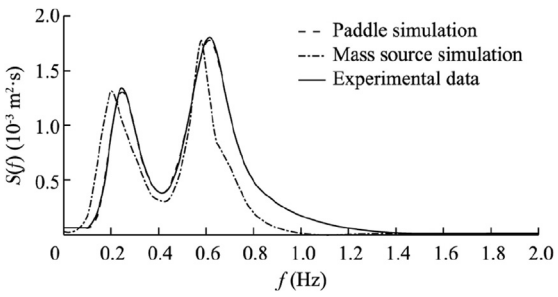

Fig. 5. Observed and simulated spectra for T_p = 21 s and P_{sc} = 30% from a 27-min simulation.

3.3.2. Mass stability

Long-duration simulations are important for understanding irregular wave conditions as they can provide more accurate results and a better representation of a desired sea state. For these simulations, each test lasted 1660 s, allowing time for any mass fluctuations to be investigated. Due to the length of the flume, any mass fluctuation that could have caused a significant increase in the water level in a smaller flume (e.g., 30 m) may not have caused such a large effect as that in the 100 m flume. Therefore, to investigate the effect any mass fluctuation has during the simulation, the average water depth along the flume was used to demonstrate the mass stability in the flume. This was done by taking a fourth-order polynomial

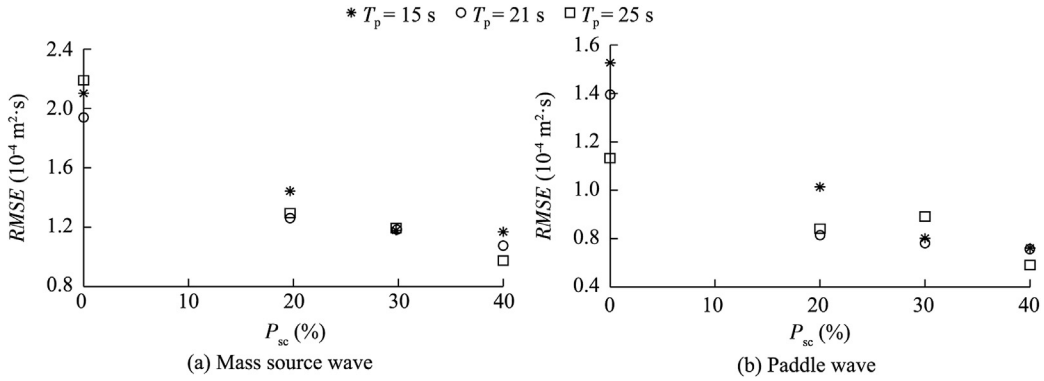

Fig. 6. *RMSE* between observed and simulated $S(f)$ for internal mass source wave and paddle wave.

of the observed time series at P8 and calculating volume change within the flume from the polynomial. Figs. 7 and 8 present the change in average water depth for T_p = 15, 21, and 25 s for the internal mass source and paddle waves, respectively. Clearly, there is a continuing increase in water depth for both wave generation methods. The internal wave maker appears to experience a larger average water depth increase across all test cases in comparison to the paddle waves.

3.3.3. Active wave absorption method

A reason for the increase in water depth shown in Figs. 7 and 8 could be the long-period (low-frequency) waves that become trapped inside the computational domain due to reflection from the shoreline and re-reflection from the wave generating boundary. An active wave absorption method for trapping long-period waves is introduced. By generating waves with equal amplitude and opposite phase to the reflected waves, the reflected wave is counteracted and absorbed. Torres-Freyermuth et al. (2010) implemented the active wave absorption method for use with the paddle. Three assumptions underlie the absorption method: all the high-frequency energy is dissipated in the surf zone; linear superposition between incident and reflected waves is valid at the generating boundary; and the low-frequency wave reflected from the

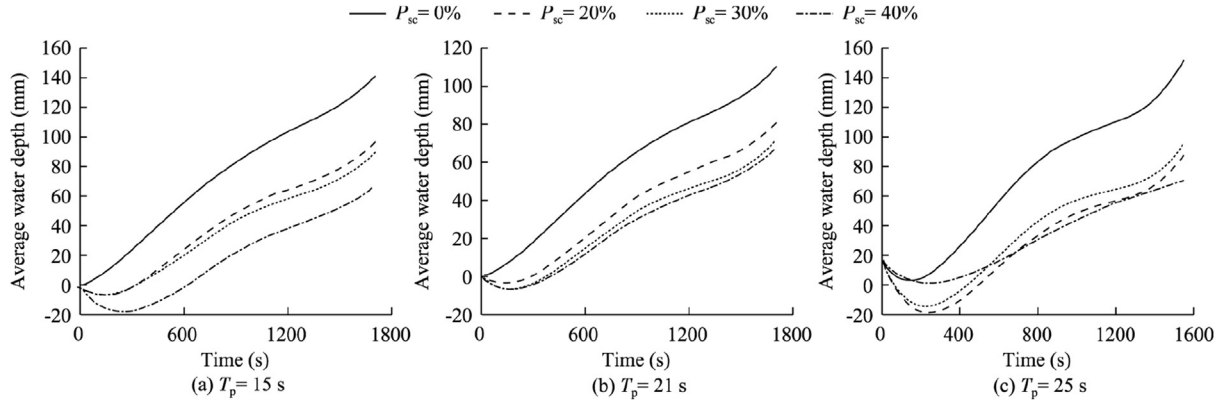

Fig. 7. Change in average water depth for internal mass source waves.

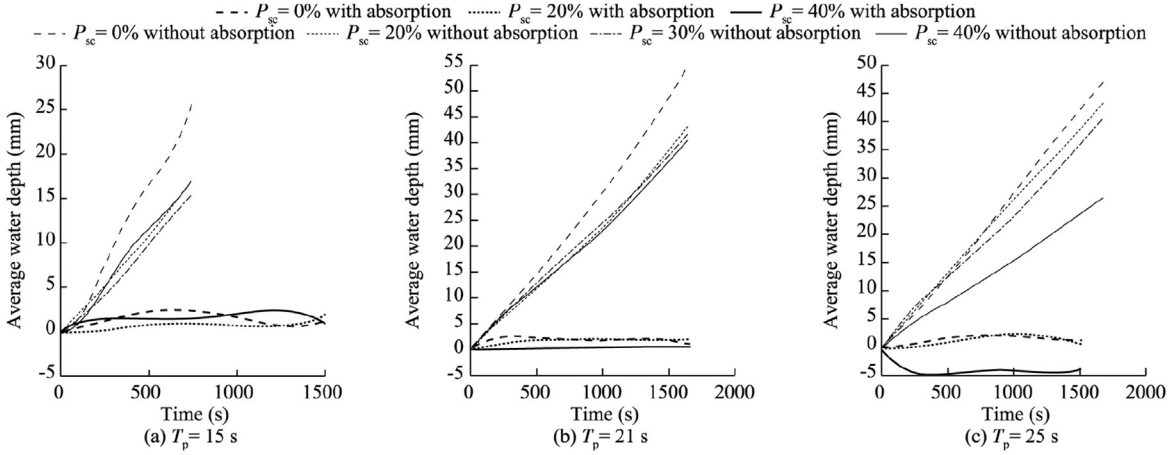

Fig. 8. Change in average water depth for paddle waves with and without active wave absorption.

shoreline propagates as a non-dispersive wave, with the speed according to the linear shallow water wave theory ($c = \sqrt{gh}$, where c is the wave speed, and h is the water depth). Therefore, the difference between the incident target-wave free-surface elevation, η_i, and the observed free-surface elevation in the numerical flume, η, at the time step m is considered the amplitude of reflected wave reaching the generating boundary:

$$\eta'^{(m+1)} = \eta_i^{(m)} - \eta^{(m)} \tag{6}$$

Assuming that the short-wave energy is completely dissipated in the surf zone, the reflected wave is therefore approximated as a non-dispersive long wave with an amplitude η'. A Sommerfeld radiation condition is then used to derive the depth-uniform horizontal velocity (Kowalik, 2003; Torres-Freyermuth, 2007):

$$u'^{(m+1)} = \eta'^{(m+1)}\sqrt{\frac{g}{h}} \tag{7}$$

The inflow boundary therefore needs to generate the incident target wave plus an additional amplitude that cancels out the reflected wave η' (Troch and De Rouck, 1999). The free-surface elevation and horizontal velocity component in the generating boundary are linearly corrected by η' and u', respectively. The updated inflow boundary condition (η_c, u_c) is then defined by

$$\eta_c^{(m+1)} = \eta_i^{(m+1)} + \eta'^{(m+1)} \tag{8}$$

$$u_c^{(m+1)} = u_i^{(m+1)} + u'^{(m+1)} \tag{9}$$

where u_i is the incident target-wave velocity.

The implementation of active wave absorption significantly improves the results, as demonstrated in Fig. 8, where the water depth only fluctuates by a maximum of 5 mm when $T_p = 25$ s and $P_{sc} = 40\%$. In comparison, using the paddle without wave absorption incurs a maximum average water depth fluctuation of 5.5 cm (at $T_p = 21$ s and $P_{sc} = 0\%$). Fluctuations do still occur, likely due to the assumptions made in the wave absorption method. The implementation of the active wave absorption method has no significant effect on wave generation, as seen in Fig. 9, which presents the *RMSE* between observed and simulated spectra; there are no significant differences in wave generation accuracy with and without active wave absorption.

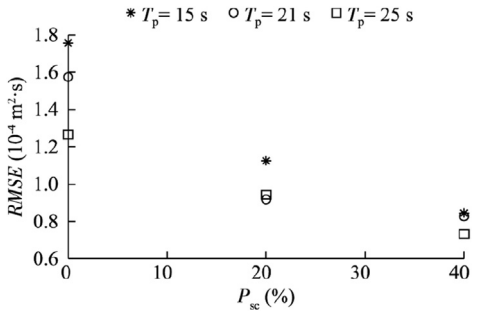

Fig. 9. *RMSE* for paddle wave generation with active wave absorption.

4. Discussion

4.1. Role of relative water depth in wave generation

In order to understand the effect of relative water depth on wave generation, systematic tests were conducted to investigate the performance of the wave generation methods in deep, intermediate, and shallow water. Linear waves were generated on a flat bottom with open boundaries, allowing waves to propagate out of the domain. The water depth was kept constant and the wave period increased to cover the range from deep to shallow water using standard definitions. A water depth of 1.708 m was used, and wave periods of 1.2 s (deep), 3.3 s (intermediate), 4.4 s (intermediate), 5.8 s (intermediate), and 8.8 s (shallow) were used to generate linear wave trains. A distance of 50 m was used from the point of wave generation to the open boundary (a 100 m total flume length for source tests) with a grid that was uniform in the x-direction with $\Delta x = 0.04$ m and non-uniform in the y-direction with a minimum spacing of $\Delta y = 0.02$ m. Fig. 10 presents the results from the paddle method, internal mass source function method, and analytical solution for linear wave generation.

The same procedure was used to investigate random waves in constant water depth, open boundaries, and varying peak wave periods to cover deep to shallow water waves. Random waves were produced by a superposition of two JONSWAP spectra to produce a time series with peak periods representing the desired wave periods (1.2, 3.3, 4.4, 5.8, and 8.8 s). Table 1 provides a breakdown of conditions generated, with the peak wind period, $T_{p,wind}$, peak swell period, $T_{p,swell}$, mean zero-crossing period, T_z, and observed peak period, T_p, for each time series. The paddle and internal mass source function methods then produced the same time series and the results were compared with the analytical solution (Fig. 11). The investigation tested not only the capabilities of the generation methods of producing random waves from deep to shallow water waves but also how well they produced significant bimodal conditions, with both low- and high-frequency waves, at varying effective water depths.

4.1.1. Wave paddle method

The wave paddle produces accurate results when compared with the analytical solutions for both the linear and random waves. It copes well with producing deep, intermediate, and shallow water waves, linearly and randomly. It is also able to replicate quick changes between high- and low-frequency waves, as presented in Fig. 11. This also supports the results seen in Figs. 5, 6(b), and 9, where higher accuracy of bimodal wave generation in comparison with the internal mass source function results is observed. Further study of the effect of the swell component percentage on wave generation on a flat bottom and open boundary would be beneficial to the increasing accuracy of generation of waves with a specific sea state for an increasing swell component percentage (Fig. 6(b)).

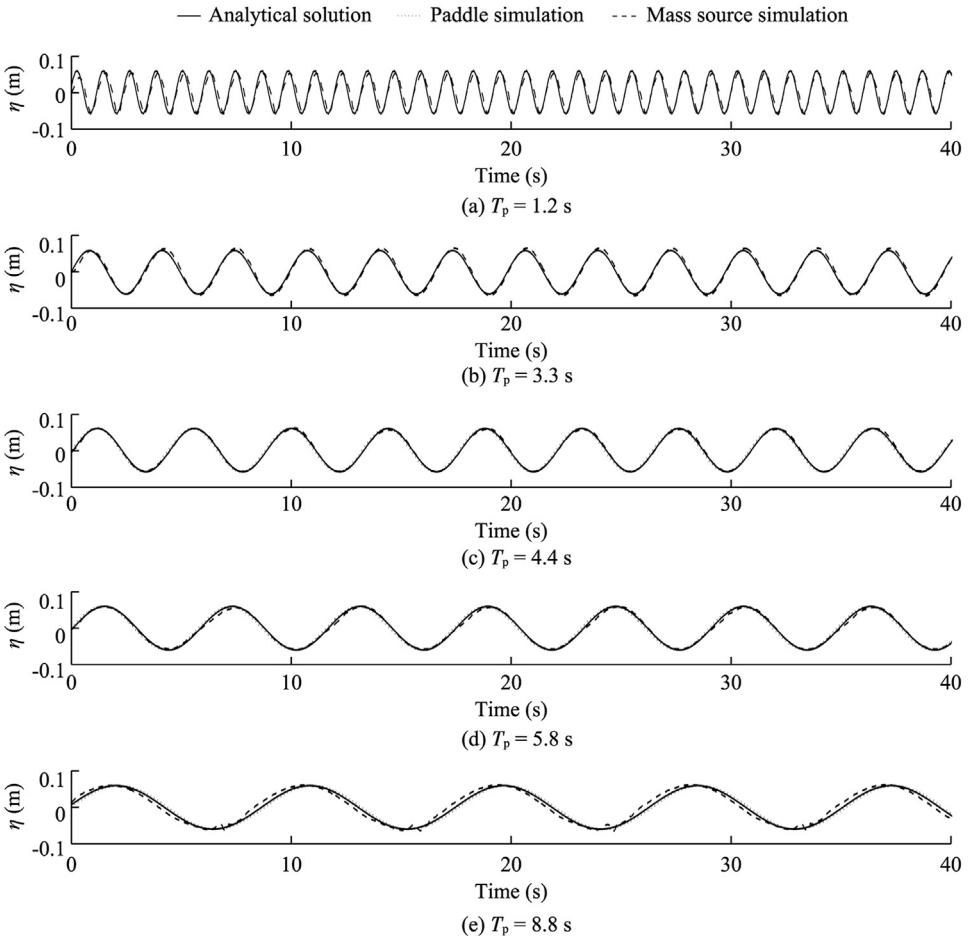

Fig. 10. Comparison between analytical solution, paddle method, and internal mass source function method for generation of linear waves.

4.1.2. Internal mass source function method

The internal mass source function method is able to replicate the linear waves accurately. However, slight discrepancies are observed with regard to the deep water waves (e.g., wave in Fig. 10(a)) due to the source wave being slightly out of phase. The internal mass source function is able to adequately reproduce the random waves. However, differences between the model and analytical solutions begin to occur for wave trains of $T_p = 4.4$ s, 5.8 s, and 8.8 s (Fig. 11). The results show that, as the peak period increases, and the rapidity of changes between low- and high-frequency waves increases, the internal mass source function method encounters difficulties in replicating the higher-frequency waves immediately after low-frequency waves. In Fig. 11, it is possible to observe that the source function wave flattens out and is able to pick out the lower-frequency waves, but not the higher frequencies in between. To investigate this, the spectrum of wave with $T_p = 8.8$ s in Fig. 11 was broken down into a few representative frequencies: lowest, peak swell, peak wind, and highest. By using the same source region setup for the 8.8-s peak period test, it is possible to detect which frequency is well simulated and which is not. In Fig. 12 it is clear that the source region is unable to produce the high-frequency wave (the wave train of $T_p = 0.55$ s). To further investigate this, two additional simulations with frequencies between the highest and peak wind frequencies were produced (Fig. 13). The waves produced still do not reach the maximum and minimum of the peaks and troughs of the analytical solution. However, improvement is seen as waves approach the peak wind frequency. One reason for this is that the source region size and depth are determined from the peak-period wavelength (section 2.2.2). As this investigation considers bimodal waves, determining the source region size from their peak period may not be sufficient as a broader range of waves is considered, involving much higher-frequency waves than the longer-period peak frequency. The present internal mass source function method has to use a source region completely below the free surface in order to maintain the mass conservation. This means that the source region needs to be sufficiently low if the wave height is large. However, the deep source region is not

Table 1
Wave characteristics for each random wave time series.

Wave time series	$T_{p,swell}$ (s)	$T_{p,wind}$ (s)	T_p (s)	T_z (s)
1	1.190	1.880	1.192	1.158
2	1.193	3.330	3.331	1.308
3	4.373	1.677	4.372	1.641
4	5.811	1.709	5.812	1.737
5	8.764	1.808	8.767	1.727

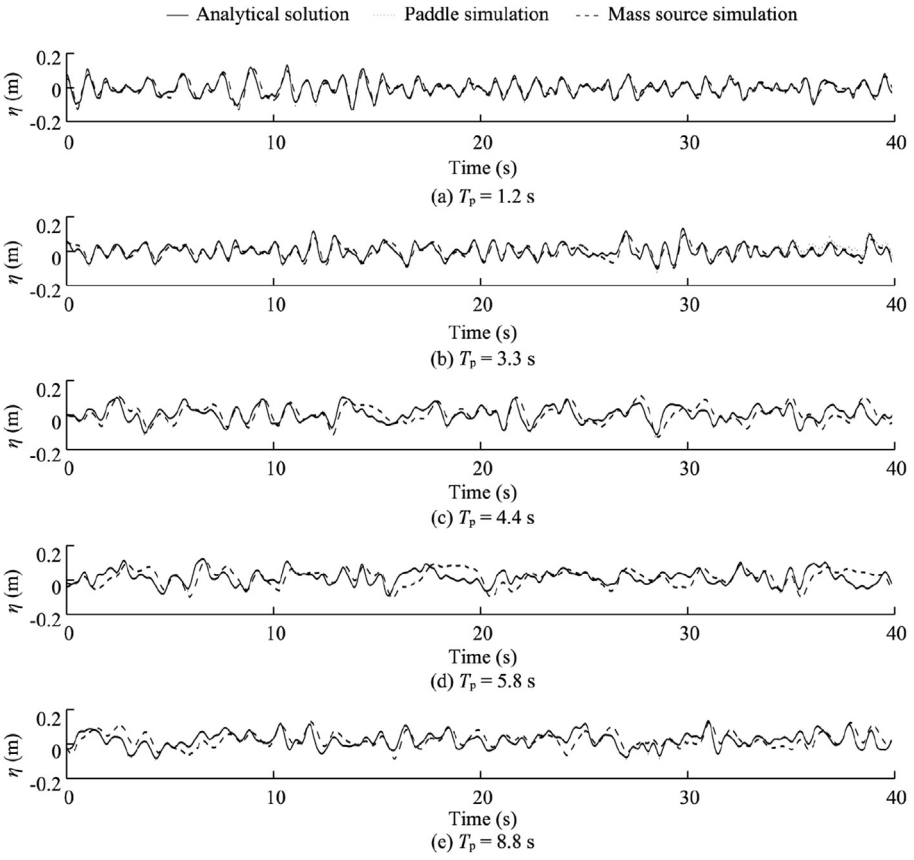

Fig. 11. Comparison between analytical solution, paddle method, and internal mass source function method for generation of bimodal waves.

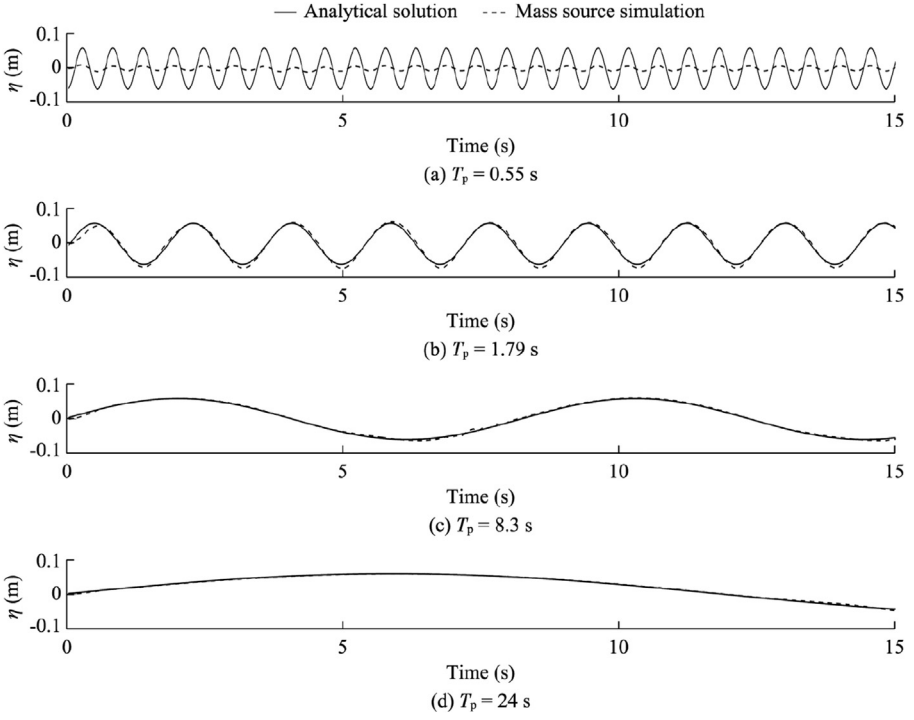

Fig. 12. Comparison between analytical solution and internal mass source function method for wave generation of representative frequencies for 8.8 s peak period spectrum.

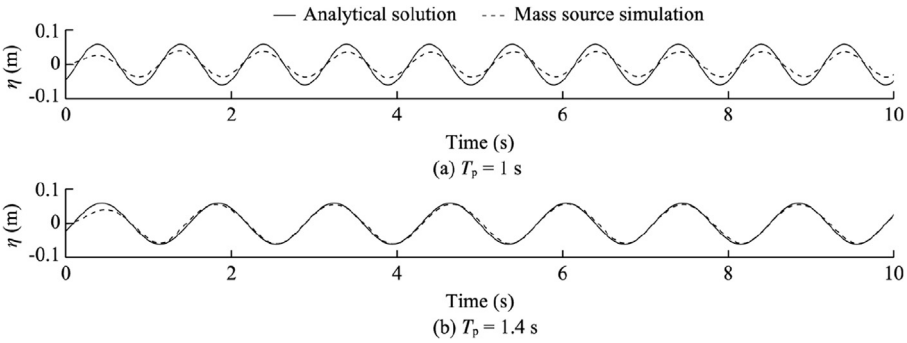

Fig. 13. Comparison between analytical solution and internal mass source function method for wave generation of frequencies between waves in Figs. 12(a) and (b).

efficient in producing high-frequency wave modes, as shown in Figs. 12 and 13. This difficulty in generating very high- and low-frequency waves supports the hypothesis behind the differences in spectra, found in Fig. 5, between the internal mass source and experimental results.

4.2. Role of beach slope in wave generation

A beach slope controls the amount of wave dissipation/reflection: a steep slope increases wave reflection, and a shallow slope increases dissipation. The data sets used in this study were based on a realistic varying beach slope, allowing for both wave breaking and reflection. A varying swell component percentage and peak period allows analysis of the effect of the beach slope on different bimodal conditions and their resulting reflection caused by the slope. The tests are significant, as both low-frequency and high-frequency waves are being produced in the flume and both wave generation methods are better at absorbing one or the other; the paddle is better at absorbing the low-frequency waves and the open boundary is better at absorbing the high-frequency waves.

4.2.1. Wave paddle method

The significance of active wave absorption is shown in Fig. 8, where results with and without wave absorption are presented. It is observed that significant increases of water depth occur without wave absorption, suggesting that wave reflection is occurring and is a key reason for the mass increase. The Stokes drift could also be a cause of the mass increase. However, the Stokes drift is deducted, as explained in section 2.2.1, from the velocity at the lateral boundary both with and without active wave absorption. The same input is used both with and without wave absorption and, therefore, it is unlikely that the Stokes drift is the main contributor to the significant increases in mass. The swell component percentage has more of an effect on the mass stability and wave generation accuracy than the peak period, as shown in Figs. 6 and 8. This is observed from the increased *RMSE* values (Fig. 6) and increased water depth changes at the lower swell component percentages (Fig. 8). This may be due to the model's capabilities of low-frequency wave generation and the tendency to over- or under-predict the low-frequency energy (Torres-Freyermuth, 2007).

4.2.2. Internal mass source function method

Mass increase is observed when the internal mass source function method is used, despite the open boundary. This has a detrimental effect on the accuracy of wave generation due to the increased water depth (Fig. 6(a)). The reasons for this include not only the reflection from the shoreline but also the wave propagation from the generation region itself. As mentioned, the open boundary is more suitable for absorbing high-frequency waves. Therefore, a bimodal sea state with a mixture of low- and high-frequency waves may not be fully absorbed. Once additional low-frequency waves begin to be reflected from the shoreline and reach the open boundary, further absorption discrepancies may occur due to the increased amount of low-frequency waves observed at the absorbing boundary.

The largest average water depth increase is greatest at a swell component percentage of 0% for both wave generation methods. A reason for this is that, for spectra with a low swell component percentage, most of the energy is contained in the high-frequency waves (Fig. 3), which are more likely to be affected by the changing water depth caused by the slope, and thus begin breaking; near-breaking waves can cause a net mass flux in the computational domain. In contrast, for spectra with a higher swell component percentage, the energy in low-frequency waves is greater, the waves are less affected by the changes in water depth, and they surge up the beach slope rather than breaking. They are therefore less likely to introduce net mass flux into the computational domain.

5. Conclusions

In this paper we have analyzed the effectiveness of two different wave generation methods in a numerical flume. Specifically, we have investigated long-period bimodal seas and an important factor often overlooked: the effect of a long computational run on accuracy of wave generation and stability of the model. Using experimental data that describe bimodal seas with increasing swell components and peak periods, comparisons have been made between the two

generation methods via comparison of power spectra and the effect of mass change on the average water depth in the flume.

In this study the wave paddle method has been able to more accurately reproduce desired wave spectra than the internal mass source function method. The swell component percentage has an effect on wave generation accuracy: a lower swell component percentage appears to generate a less accurate desired sea state. The addition of active wave absorption significantly improved the mass stability of the model. However, an increase of the water depth is still observed and therefore further testing and improvements are required to improve wave absorption and the stability of the model. Further improvement of the internal mass source function method so that it is more efficient in generating short waves could also lead to better performance in generating combined swell-wind conditions. Improvements of previous mass source random wave generation methods have been suggested, allowing for better spectra-specific wave generation by using varying frequency bands. On the basis of our results, it is suggested that the wave paddle method with active wave absorption is preferable to the internal mass source function method in investigations of intermediate-depth long-period bimodal seas for long-duration simulations.

Acknowledgements

This work was undertaken as part of the Ensemble Estimation of Flood Risk in a Changing Climate (EFRaCC) project funded by the British Council under its Global Innovation Initiative. The authors acknowledge Andrea Polidoro and Standing Conference on Problems Associated with the Coastline (SCOPAC) for providing the data sets and supplementary information, and Professor Peng-zhi Lin at Sichuan University for supplying the NEWRANS code.

References

Draper, L., Bownass, T., 1982. Unusual waves on European coasts, February 1979. Coast. Eng. Proc. 18, 270−281. http://dx.doi.org/10.1061/9780872623736.018.

Frigaard, P., Brorsen, M., 1995. A time-domain method for separating incident and reflected irregular waves. Coast. Eng. 24(3−4), 205−215. http://dx.doi.org/10.1016/0378-3839(94)00035-V.

Hafsia, Z., Haj, M.B., Lamloumi, H., Maalel, K., 2009. Comparisons between moving paddle and mass source methods for solitary wave generation and propagation over a steep sloping beach. Eng. Appl. Comput. Fluid Mech. 3(3), 355−368. http://dx.doi.org/10.1080/19942060.2009.11015276.

Higuera, P., Lara, J.L., Losada, I.J., 2013. Realistic wave generation and active wave absorption for Navier-Stokes models. Application to OpenFOAM. Coast. Eng. 71, 102−118. http://dx.doi.org/10.1016/j.coastaleng.2012.07.002.

Jones, D.K., Zou, Q., Reeve, D.E., 2013. Computational modelling of coastal flooding caused by combined surge overflow and wave overtopping on embankments. J. Flood Risk Manag. 6(2), 70−84. http://dx.doi.org/10.1111/j.1753-318X.2012.01155.x.

Kowalik, Z., 2003. Basic relations between Tsunamis calculation and their physics−II. Sci. Tsunami Hazards 21(3), 154−173.

Lara, J.L., Garcia, N., Losada, I.J., 2006. RANS modelling applied to random wave interaction with submerged permeable structures. Coast. Eng. 53(5−6), 395−417. http://dx.doi.org/10.1016/j.coastaleng.2005.11.003.

Lara, J.L., Ruju, A., Losada, I.J., 2010. Reynolds averaged Navier-Stokes modelling of long waves induced by a transient wave group on a beach. Proc. R. Soc. A Math. Phys. Eng. Sci. 467(2129), 1215−1242. http://dx.doi.org/10.1098/rspa.2010.0331.

Lin, P.Z., Liu, P.L.-F., 1998. A numerical study of breaking waves in the surf zone. J. Fluid Mech. 359, 239−264. http://dx.doi.org/10.1017/S002211209700846X.

Lin, P.Z., Liu, P.L.-F., 1999. Internal wave-maker for Navier-Stokes equations models. J. Waterw. Port. Coast. Ocean Eng. 125(4), 207−215. http://dx.doi.org/10.1061/(ASCE)0733-950X(1999)125:4(207).

Reeve, D.E., Soliman, A., Lin, P.Z., 2008. Numerical study of combined overflow and wave overtopping over a smooth impermeable seawall. Coast. Eng. 55(2), 155−166. http://dx.doi.org/10.1016/j.coastaleng.2007.09.008.

Shih, T., Zhu, J., Lumley, J.L., 1996. Calculation of wall-bounded complex flows and free shear flows. Int. J. Numer. Methods Fluids 23(11), 1133−1144. http://dx.doi.org/10.1002/(SICI)1097-0363(19961215)23:11<1133::AID-FLD456>3.0.CO;2-A.

Sibley, A., Cox, D., 2014. Flooding along English Channel coast due to long-period swell waves. Weather 69(3), 59−66. http://dx.doi.org/10.1002/wea.2145.

Slingo, J., Belcher, S., Scaife, A., McCarthy, M., 2014. The Recent Storms and Floods in the UK. Met Office, Exeter. http://www.metoffice.gov.uk/research/news/2014/uk-storms-and-floods [Retrieved Feb. 22, 2015].

Soliman, A., 2003. Numerical Study of Irregular Wave Overtopping and Overflow. Ph.D. Dissertation. Nottingham University, Nottingham.

Torres-Freyermuth, A., 2007. Estudio de la Hidrodin'amica de la Zona de Rompientes mediante ecuaciones tipo RANS. Ph. D. Dissertation. University of Cantabria, Santander.

Torres-Freyermuth, A., Losada, I.J., Lara, J.L., 2007. Modeling of surf zone processes on a natural beach using Reynolds-Averaged Navier-Stokes equations. J. Geophys. 112(C9), C09014. http://dx.doi.org/10.1029/2006JC004050.

Torres-Freyermuth, A., Lara, J.L., Losada, I.J., 2010. Numerical modelling of short- and long-wave transformation on a barred beach. Coast. Eng. 57(3), 317−330. http://dx.doi.org/10.1016/j.coastaleng.2009.10.013.

Troch, P., De Rouck, J., 1999. An active wave generating-absorbing boundary condition for VOF type numerical model. Coast. Eng. 38(4), 223−247. http://dx.doi.org/10.1016/S0378-3839(99)00051-4.

Turton, J., Fenna, P., 2008. Observations of extreme wave conditions in the north-east Atlantic during December 2007. Weather 63(12), 352−355. http://dx.doi.org/10.1002/wea.321.

Wei, G., Kirby, J.T., Sinha, A., 1999. Generation of waves in Boussinesq models using a source function method. Coast. Eng. 36(4), 271−299. http://dx.doi.org/10.1016/S0378-3839(99)00009-5.

Zou, Q.P., Chen, Y.P., Cluckie, I., Hewston, R., Pan, S.Q., Peng, Z., Reeve, D.E., 2013. Ensemble prediction of coastal flood risk arising from overtopping by linking meteorological, ocean, coastal and surf zone models. Q. J. R. Meteorol. Soc. 139(671), 298−313. http://dx.doi.org/10.1002/qj.2078.